ISSN 1674-1056
http://cpb.iphy.ac.cn
http://iopscience.iop.org/cpb
中国物理 B
Chinese Physics
中国物理
Chinese Physics B

Excited state intramolecular proton transfer mechanism of o-hydroxynaphthyl phenanthroimidazole

Shuang Liu(刘爽)[1], Yan-Zhen Ma(马艳珍)[2], Yun-Fan Yang(杨云帆)[2], Song-Song Liu(刘松松)[1], Yong-Qing Li(李永庆)[2], Yu-Zhi Song(宋玉志)[1]
Citation: Chin. Phys. B . 2018, 27(2): 023103. **doi:** 10.1088/1674-1056/27/2/023103

Journal homepage: http://cpb.iphy.ac.cn; http://iopscience.iop.org/cpb

What follows is a list of articles you may be interested in

Structural stability of ultra-high temperature refractory material $MoSi_2$ and Mo_5Si_3 under high pressure

Hao Liang(梁浩), Fang Peng(彭放), Cong Fan(樊聪), Qiang Zhang(张强), Jing Liu(刘景), Shi-Xue Guan(管诗雪)
Chin. Phys. B . 2017, 26(5): 053101. **doi:** 10.1088/1674-1056/26/5/053101

Ab initio path-integral molecular dynamics and the quantum nature of hydrogen bonds

Yexin Feng(冯页新), Ji Chen(陈基), Xin-Zheng Li(李新征), Enge Wang(王恩哥)
Chin. Phys. B . 2016, 25(1): 013104. **doi:** 10.1088/1674-1056/25/1/013104

Theoretical study of *γ*-aminobutyric acid conformers： Intramolecular interactions and ionization energies

Wang Ke-Dong, Wang Mei-Ting, Meng Ju
Chin. Phys. B . 2014, 23(10): 103101. **doi:** 10.1088/1674-1056/23/10/103101

Further investigations of the low-lying electronic states of AsO^+ radical

Zhu Zun-Lue, Qiao Hao, Lang Jian-Hua, Sun Jin-Feng
Chin. Phys. B . 2013, 22(10): 103102. **doi:** 10.1088/1674-1056/22/10/103102

Density functional study of uranyl (VI) amidoxime complexes

Chi Fang-Ting, Li Peng, Xiong Jie, Hu Sheng, Gao Tao, Xia Xiu-Long, Wang Xiao-Lin
Chin. Phys. B . 2012, 21(9): 093102. **doi:** 10.1088/1674-1056/21/9/093102

Excited state intramolecular proton transfer mechanism of o-hydroxynaphthyl phenanthroimidazole*

Shuang Liu(刘爽)[1], Yan-Zhen Ma(马艳珍)[2], Yun-Fan Yang(杨云帆)[2], Song-Song Liu(刘松松)[1], Yong-Qing Li(李永庆)[2,†], and Yu-Zhi Song(宋玉志)[1,‡]

[1] School of Physics and Electronics, Shandong Normal University, Jinan 250014, China
[2] Department of Physics, Liaoning University, Shenyang 110036, China

(Received 10 October 2017; revised manuscript received 22 November 2017; published online 29 January 2018)

By utilizing the density functional theory (DFT) and the time-dependent density functional theory (TDDFT), the excited state intramolecular proton transfer (ESIPT) mechanism of o-hydroxynaphthyl phenanthroimidazole (HNPI) is studied in detail. Upon photo is excited, the intramolecular hydrogen bond is obviously enhanced in the S_1 state, which thus promotes the ESIPT process. Hydrogen bond is shown to be strengthened via comparing the molecular structures and the infrared vibration spectra of the S_0 and S_1 states. Through analyzing the frontier molecular orbitals, we can conclude that the excitation is a type of the intramolecular charge transfer excitation, which also indicates the trend of proton transfer in S_1 state. The vertical excitation based on TDDFT calculation can effectively repeat the absorption and fluorescence spectra of the experiment. However, the fluorescence spectrum of normal structure, which is similar to the spectrum of isomer structure is not detected in the experiment. It can be concluded that the fluorescence measured in the experiment is attributed to both structures. In addition, by analyzing the potential energy curves (PECs) calculated by the B3LYP functional method, it can be derived that since the molecule to cross the potential barrier in the S_1 state is smaller than in the S_0 state and the reverse proton transfer process in the S_1 state is more difficult than in the S_0 state, the ESIPT occurs in the S_1 state.

Keywords: hydrogen bond, ESIPT, RDG, PECs

PACS: 31.15.ae, 31.15.A–, 31.15.es **DOI:** 10.1088/1674-1056/27/2/023103

1. Introduction

As one of the cases of most important weak interactions, hydrogen bond plays quite a vital role in the study of photochemistry, such as supramolecular photochemistry, material photochemistry, biochemistry, and photochemistry of solution, etc.[1–5] Since the pioneering work by Weller *et al.*,[6,7] the excited state intra- and inter-molecular proton transfer (ESIPT) have become a research focus in experiment and in theory.[1,2,8–11] For example, Zhao *et al.* have been deciphered the excited state behavior for 2- (4′-N, N-dimethylaminophenyl) imidazo [4, 5-b] pyridine.[12] Specifically, Han *et al.*[13–18] first reported that the hydrogen bond was strengthened on a 200-fs time scale, which broke the commonly accepted hydrogen bond dissociation mechanism, and proposed the strengthening mechanism of hydrogen bonding by studying excited state proton transfer.[10,11] Once a molecule is excited to the lowest excited state (enol* form) from the ground state (enol form), the hydrogen bond is first enhanced, proton will transfer between proton acceptor and donor through intra- or inter-molecular hydrogen bond. Then, the keto* form becomes the ground-state keto structure by emitting a longer wavelength fluorescence.[19–21] Finally ground-state keto form transfers back to the ground-state enol species via a reverse ground-state proton transfer process, which constitutes a four-level reaction cycle. The ESIPT thus possesses different photophysical and photochemical properties providing various applications in some areas, such as in luminescent materials, metal ion sensors, fluorescent probes, photonabilium, laser fuels, UV filters, light-emitting diodes, molecular switches, photostabilization, radiation hard-scintillator counters, organic light emitting devices (OLEDs), etc.[22–28]

Since the phenanthroimidazole derivatives have good molecular structural characteristics, they have aroused the great research interest of researchers. By using the TiO_2(R) nano-semiconductor as the catalyst under solventless condition, Jayabharathi *et al.*[29] synthesized five phenanthroimidazole derivatives, which were then characterized via nuclear magnetic resonance (NMR) and single crystal x-ray diffraction (XRD) techniques. Shahid and Misra[30] synthesized three molecular systems based phenanthroimidazole moiety and studied photo enolization via ESIPT mechanism. The results revealed that the o-hydroxynaphthyl phenanthroim-

*Project supported by the Shandong Provincial Higher Educational Science and Technology Program, China (Grant No. J17KA186), the Taishan Scholar Project of Shandong Province, China, the Natural Science Foundation of Liaoning Province, China (Grant No. 20170540408), and the Science and Technology Plan Project of Shenyang City, China (Grant No. 17-231-1-06).

†Corresponding author. E-mail: yqli@lnu.edu.cn
‡Corresponding author. E-mail: yzsong@sdnu.edu.cn

© 2018 Chinese Physical Society and IOP Publishing Ltd

idazole (HNPI) and o-hydroxyphenyl phenanthroimidazole (HPPI) show light triggered enolization. However, benzyl phenanthroimidazole (BPNI) could not show the phenomenon of proton transfer due to the absence of OH moiety. Specifically, fluorescence "turn-off" and "turn-on" behavior could occur when HNPI interacts with AcO^-, which thus could be used as a probe of AcO^-.

Although Shahid and Misra[30] experimentally studied in detail the photo enolization process of HNPI triggered by the ESIPT mechanism, they obtained only the geometry optimization and frontier molecular orbital by quantum chemical calculation, which cannot be quantitatively nor qualitatively explain the ESIPT mechanism. Thus we are motivated to carry out a clear and detailed theoretical investigation on ESIPT of HNPI by utilizing DFT and TDDFT methods.[31] We study the excited state dynamical process of HNPI by performing detailed calculation on the properties of both the ground and excited states, such as the geometry optimization, potential energy curves, the frontier molecular orbital, reduced density gradient (RDG), IR spectrum, absorption and emission spectra, etc. We investigate the ESIPT mechanism of HNPI in detail, which is not only to clarify excited state dynamical process of HNPI system, but also to facilitate the understanding of intramolecular hydrogen bond dynamical processes.

The rest of this paper is organized as follows. In Section 2 we describe the computational details used in the present work. In Section 3, we describe in detail the results and discussion. The final remarks of the current work are presented in Section 4.

2. Computational details

The S_0 and S_1 state optimizations of HNPI molecule are carried out by using the DFT and TDDFT methods, which are implemented in the Gaussian 09 program suite.[31] B3LYP[32] functional and 6-31+G (d) basis set[33] are employed in both the DFT and TDDFT calculations. In order to simulate the environment of the acetonitrile solvent, the polarizable continuum model (PCM) and integral equation formalism variant PCM (IEFPCM)[34–37] are employed in the present work, which can reproduce the experimental results well. All the bond lengths, bond angles and dihedral angles are relaxed in the optimization of HNPI molecule in S_0 and S_1 states. In order to verify the structures corresponding to local minima in S_0 and S_1 states, the vibrational frequencies are calculated, which give no imaginary frequency. By using the optimized geometry of ground-state HNPI molecule, the vertical excitations are obtained by TDDFT calculation considering ten low-lying electronic states.[1,16,18,38–42] The PECs of S_0 and S_1 states are scanned,[43] which follows a constrained optimization by varying O–H bond length in the enol form ranging from 0.9 Å to 1.9 Å in steps of 0.03 Å. The vibration frequencies are determined via the diagonalization of the Hessian matrix. The gradients of dipole moment are utilized to determine the infrared (IR) intensity. In order to distinguish among the different types of interactions in HNPI molecule, the reduced density gradient (RDG) is calculated using Multiwfn.[44] Such as RDG is then visualized, from which the hydrogen bond can be easily recognized.

3. Results and discussion

3.1. Optimization of HNPI

The enol and keto forms are optimized employing DFT and TDDFT methods in ground (S_0) and excited (S_1) states of HNPI, respectively, which is subsequently followed by vibrational frequency analysis in order to validate such stationary points. The optimized enol and keto structures in ground state are shown in Fig. 1. For illustrating the change of hydrogen bond more clearly and concisely, the atoms related to hydrogen bond are marked with serial numbers as shown in Fig. 1. The corresponding bond lengths and bond angles of HNPI are listed in Table 1. For the enol form, it can be seen from Table 1 that O_1–H_2 bond length is 0.998 Å in S_0 state, which increases to 1.001 Å in the first excited state (S_1). In the meanwhile, the H_2–N_3 bond length decreases from 1.727 Å to 1.692 Å, and the O_1-$H_2 \cdots N_3$ bond angle increases from 146.8° to 147.7°. The decrease of the H_2–N_3 bond length and the increase of the O_1–H_2 bond length as well as the increase of bond angle O_1-$H_2 \cdots N_3$ in the S_1 state lead to the hydrogen bonding

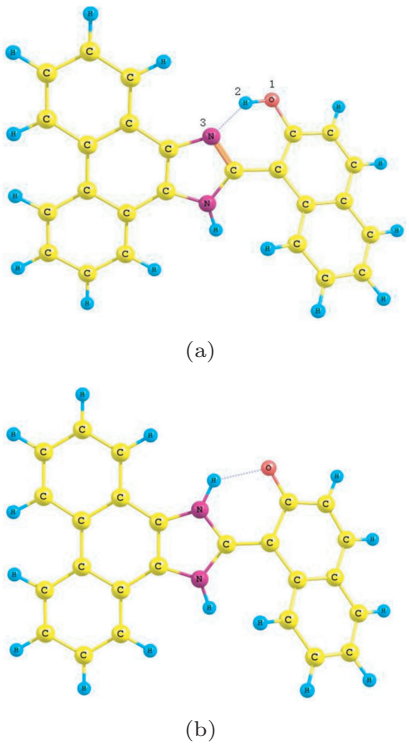


Fig. 1. (color online) Optimized structures of HNPI molecules of enol and keto forms in S_0 state: blue: H, yellow: C, red: O, pink: N. The dash line refers to the intramolecular hydrogen bond.

Table 1. Primary optimized bond lengths (in unit Å) and bond angles (°) of hydrogen bond groups for normal form (enol) and tautomeric forms (keto) of the HNPI in S_0 and S_1 states.

	Enol		Keto	
	S_0	S_1	S_0	S_1
O_1–H_2	0.998	1.001	1.726	1.843
H_2–N_3	1.727	1.692	1.036	1.026
$\sigma(O_1$–H_2–$N_3)$	146.8°	147.7°	133.2°	128.9°

enhancement. For the keto form, the O_1–H_2 bond length increases by 0.117 Å from S_0 state to S_1 state. While the H_2–N_3 bond length and $O_1 \cdots H_2$–N_3 bond angle decrease by 0.01 Å and 4.3°, respectively. It can also be concluded that the hydrogen bond in the S_0 state is stronger than in S_1 state.

A clear-cut feature of hydrogen bond dynamics can be obtained by analyzing the vibrational frequency of O_1–H_2 moiety which is related to the O_1–$H_2 \cdots N_3$. It is well known that IR spectrum is an effective method to determine whether the proton transfer occurs, which is judged by the blue shift or red shift of the IR spectrum.[45] Thus, the IR spectra of HPNI in enol form are calculated both for the S_0 state and for the S_1 state, which is shown in Fig. 2. The O_1–H_2 stretching vibrational frequency in S_0 state is calculated to be 3165 cm^{-1}, which then becomes 3079 cm^{-1} when HPNI is excited to S_1 state, showing a red shift of 86 cm^{-1}. The red shift of O_1–H_2 stretching vibrational frequency also shows that the intramolecular hydrogen bond O_1–$H_2 \cdots N_3$ is reinforced in S_1 state.

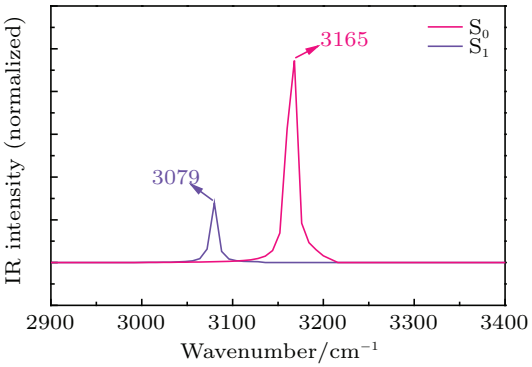


Fig. 2. (color online) IR spectra of enol-form HPNI at the spectral region of the O_1–H_2 stretching band in the S_0 and S_1 states.

3.2. Frontier molecular orbital (MO) analyses

The frontier molecular orbitals (mainly the highest occupied molecular orbital (HOMO) and the lowest unoccupied molecular orbital (LUMO)) are calculated and analyzed for better understanding the charge distribution and charge transfer in the HNPI molecule. In Fig. 3, we display the calculated HOMO and LUMO of the HPNI molecule in the enol form. The calculated electronic transition energies, oscillator strengths and compositions are listed in Table 2. The oscillator strength of the first excited state is calculate to be 0.6050 with the orbital contribution being 97.94%, which is much larger than those of the second and third excited states. It can be seen from Fig. 3 that the HOMO displays π feature, while the LUMO exhibits π^* feature, thus the transition of two orbitals shows $\pi\pi^*$ character in the first excited state, it can also be observed that the electron distributions in HOMO and LUMO are different from each other. The electron distribution of O_1–H_2 bond is reduced, whereas the electron distribution of the N_3 atom is increased, which strengthens the hydrogen bonding and promotes the ESIPT process.[46,47] In addition, the electron population of the HOMO is distributed on the whole molecule, while the electrons of LUMO are distributed mainly only on the right moiety, which exhibits a distinct intramolecular charge transfer (ICT). Thus, we can conclude that the excitation type belongs to intramolecular charge transfer excitation.

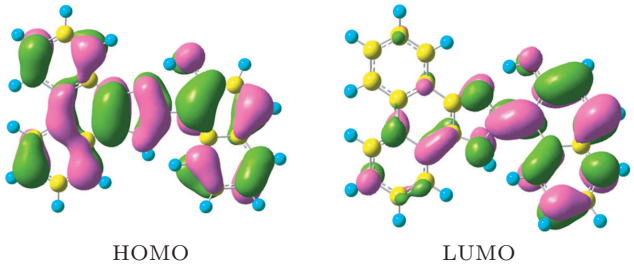


Fig. 3. (color online) Visual electron population of the frontier molecular orbitals HOMO and LUMO.

Table 2. Excitation wavelengths, oscillator strengths and the corresponding orbital transition contributions of HNPI molecule.

Transition	λ/nm	f	Composition	CI/%
$S_0 \rightarrow S_1$	378.88	0.605	H→L	97.94
$S_0 \rightarrow S_2$	345.12	0.0042	H-1→L	90.88
$S_0 \rightarrow S_3$	322.92	0.0579	H-2→L	86.00

3.3. Absorption and emission spectra

The absorption and fluorescence spectra of HNPI molecule are displayed in Fig. 4 with wavelengths ranging from 200 nm to 800 nm. The peaks of calculated absorption spectra are located at 378.8 nm, which is consistent with the experiment result[48] 370 nm, showing a minor difference of 8.8 nm. As for the emission spectra, the peak of keto* form is calculated to be 482.1 nm which is 35.9 nm smaller than the experimental result.[48] The fluorescence spectrum of enol* form at 476.2 nm which is similar to the keto* form is not detected in the experiment, thus the fluorescence measured in the experiment is attributed to both structures. The consistence between the absorption and emission peaks ensures the validity of the method employed in the present work. The abnormal change of photophysical property is very often along with tremendous change in molecular structure compared with in normal structure. Abnormal change in the optical characteristic is often accompanied by a huge change in the molecular

structure compared with in the normal structure. Therefore, we can conclude that the change in Stokes shift reflects the change in photophysical property.

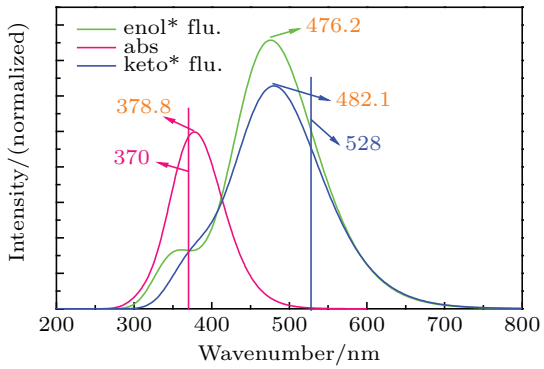


Fig. 4. (color online) Absorption (abs) and fluorescence (flu.) spectra of HNPI, obtained at the calculated level of B3LYP/6-31+G (d)/IEF-PCM (acetonitrile).

3.4. Potential energy curves

For a more comprehensive understanding of the process that the proton migrates from the hydroxyl group to nitrogen atom, we plot in Fig. 5 that the PECs as a function of O_1–H_2 bond ranging from 0.9 Å to 1.9 Å in steps of 0.03 Å. It can be derived from Fig. 5 that the proton transfer may overcome a potential barrier about 5.76 kcal/mol in the S_0 state, which is slightly bigger than that in S_1 state (5.12 kcal/mol). However, the reverse proton transfer immediately occurs after proton transfer. The potential barrier of reversed proton transfer is 2.2 kcal/mol in the S_0 state, which is much smaller than that of S_1 state (4.28 kcal/mol), thus it is unstable and returns to the enol form quickly. This demonstrates that the reversed proton transfer process is more difficult to occur in the S_1 state than in the S_0 state. Subsequently, keto* form returns to ground-state keto form via radiation fluorescence.

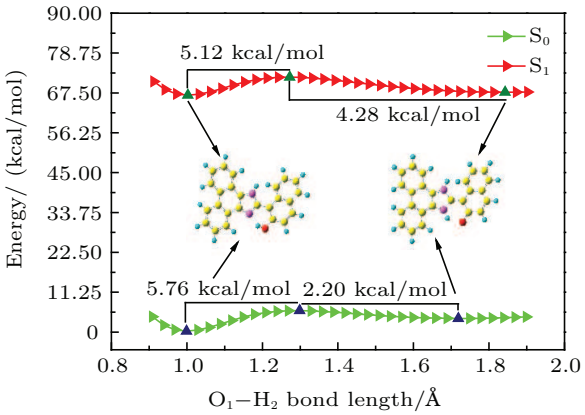


Fig. 5. (color online) Curves of potential energy versus O_1–H_2 bondlength in a frequency range from 0.9 Å to 1.9 Å of the HNPI molecule in S_0 and S_1 states.

3.5. Discriminating weak interaction types by filling color to RDG isosurfaces

By combining the RDG function and the $\rho(r)$ function, we can distinguish between the type and intensity of weak interaction.[49] The equation can be expressed as

$$\mathrm{RDG}(r) = \frac{1}{2(3\pi^2)^{1/3}} \frac{|\nabla\rho(r)|}{\rho(r)^{4/3}}, \tag{1}$$

$$\Omega(r) = \mathrm{Sign}(\lambda_2(r))\rho(r), \tag{2}$$

where RDG is the reduced density gradient and $\rho(r)$ is the total electron density. According to atom in molecule (AIM) theory,[50] the relationship between the second largest eigenvalue λ_2 and $\rho(r)$ of the electron density Hessian matrix as shown in Eq. (2), $\rho(r)$ is an important measure of weak interaction intensity, while the type of weak interaction is represented by the sign (λ_2) function. Therefore, the weak interactions of different types can be analyzed by drawing the scatter graph of function 1 (RDG) and function 2 ($\Omega(r)$). The function obtained by multiplying the function of $\rho(r)$ and sign (λ_2) and thus yielding the RDG isosurface is shown in Fig. 6(a) with a contour value of 0.5 and the RDG isosurface ranging from −0.04 to 0.02. The spike of the hydrogen bond is located at −0.036 a.u., which indicates that the hydrogen bond is extremely strong in the S_1 state. Similarly, the weak interactions can be distinguished in Fig. 6(b). It can be explicitly observed from Fig. 6(b) that there is a strong hydrogen bond between O_1–$H_2 \cdots N_3$.

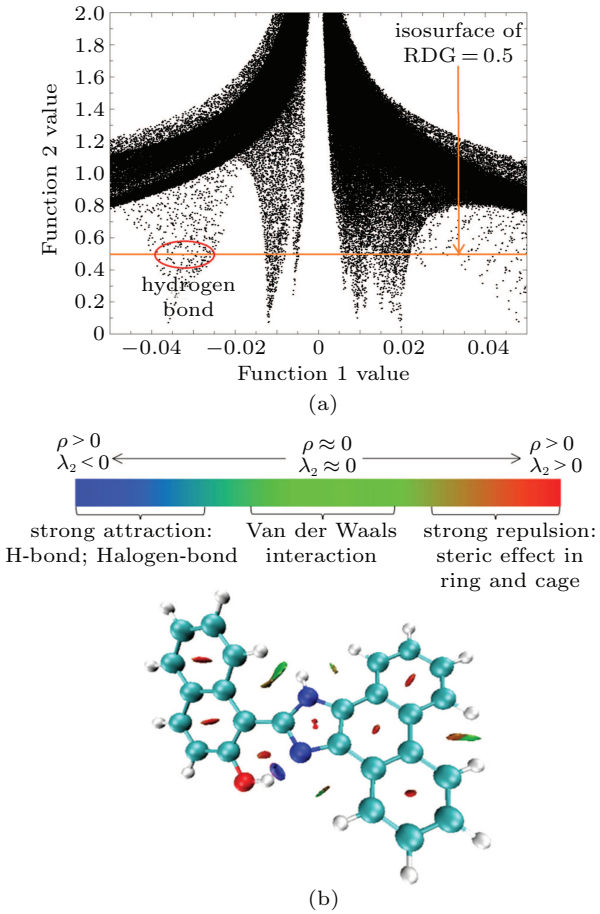


Fig. 6. (color online) (a) Plot of reduced density gradient (RDG) versus $\Omega(r)$ for function value 1 and function value 2. (b) Different types of weak interactions represented by different color gradients as well as RDG isometric surfaces.

4. Conclusions and perspectives

The DFT/TDDFT/B3LYP functional method is utilized to study the ESIPT mechanism of HNPI molecule. We can conclude that the proton transfer occurs in the S_1 state via analyzing the calculated electron spectrum, infrared spectrum and potential energy curves. In addition, by analyzing the bond lengths, bond angles and the frontier molecular orbitals in the S_0 state and the S_1 state, respectively, we can prove that the hydrogen bond interaction can be strengthened, which plays a decisive role in proton transfer. In addition, we carry out a detailed study of the proton transfer process of HNPI molecule by calculating the PECs of S_0 and S_1 states. The obtained potential barriers of reversed proton transfer are 4.28 kcal/mol in the S_1 state and 2.2 kcal/mol in the S_0 state, respectively. Thus it can be concluded that the reverse proton transfer process in the S_0 state is more difficult than in the S_1 state. Therefore, we can derive from the above analysis that the proton transfer occurs in the S_1 state, which is of great significance for doing molecular research.

References

[1] Zhao G J and Han K L 2008 *J. Comput. Chem.* **29** 2010
[2] Zhao G J, Han K L and Stang P J 2009 *J. Chem. Theory Comput.* **5** 1955
[3] Zhao G J and Han K L 2008 *Biophys. J.* **94** 38
[4] Zhao G J and Han K L 2010 *Phys. Chem. Chem. Phys.* **12** 8914
[5] Zhou P, Song P, Liu J, Han K and He G 2009 *Phys. Chem. Chem. Phys.* **11** 9440
[6] Weller A and Elektrochem Z 1956 *Phys. Chem.* **60** 1144
[7] Weller A 1955 *Naturwissenschaften* **42** 175
[8] Han K L, He G Z and Lou N Q 1996 *J. Chem. Phys.* **105** 8699
[9] Li D, Huang X, Han K and Zhan C G 2011 *J. Am. Chem. Soc.* **133** 7416
[10] Yang Y, Zhao J and Li Y 2016 *Sci. Rep. UK* **6** 32152
[11] Zhang Y, Sun M and Li Y 2016 *Sci. Rep. UK* **6** 25568
[12] Zhao J, Liu X and Zheng Y 2017 *J. Lumin.* **188** 1
[13] Zhao G J and Han K L 2007 *J. Chem. Phys.* **127** 024306
[14] Chai S *et al.* 2009 *Phys. Chem. Chem. Phys.* **11** 4385
[15] Zhao G J, Liu Y H, Han K L and Dou Y 2008 *Chem. Phys. Lett.* **453** 29
[16] Zhao G J and Han K L 2012 *Acc. Chem. Res.* **45** 404
[17] Zhao G J and Han K L 2007 *J. Phys. Chem. A* **111** 2469
[18] Zhao G J, Han K L, Lei Y B and Dou Y S 2007 *J. Chem. Phys.* **127** 415
[19] Song P and Ma F C 2013 *Int. Rev. Phys. Chem.* **32** 589
[20] Demchenko A P, Tang K C and Chou P T 2013 *Chem. Soc. Rev.* **42** 1379
[21] Tseng H W *et al.* 2015 *J. Phys. Chem. Lett.* **6** 1477
[22] Chen J S, Zhou P W, Yang S Q, Fu A P and Chu T S 2013 *Phys. Chem. Chem. Phys.* **15** 16183
[23] Yu F, Li P, Wang B and Han K 2013 *J. Am. Chem. Soc.* **135** 7674
[24] Ji E K and Park S Y 2011 *Adv. Mater.* **23** 3615
[25] Tang K C *et al.* 2011 *J. Am. Chem. Soc.* **133** 17738
[26] P S S, J G, Y P T and E V 2009 *J. Phys. Chem. B* **113** 4953
[27] Li Y, Xu B, Song P, Ma F C and Sun M 2017 *J. Phys. Chem. C* **121** 12546
[28] Xu B, Li Y, Peng S, Ma F and Sun M 2017 *Sci. Rep. UK* **7** 45688
[29] Jayabharathi J, Ramanathan P and Thanikachalam V 2014 *New J. Chem.* **39** 142
[30] Shahid M and Misra A 2016 *J. Photoch. Photobio. A* **335** 190
[31] Frisch M J *et al.* 2009 Gaussian 09, Revision A.02, Gaussian, Inc. Wallingford CT
[32] Lee C, Yang W and Parr R G 1988 *Phys. Rev. B* **37** 785
[33] Rassolov V A, Ratner M A, Pople J A, Redfern P C and Curtiss L A 2001 *J. Comput. Chem.* **22** 976
[34] Cammi R and Tomasi J 1995 *J. Comput. Chem.* **16** 1449
[35] Cancès E, Mennucci B and Tomasi J 1997 *J. Chem. Phys.* **107** 3032
[36] Johnson E R *et al.* 2010 *J. Am. Chem. Soc.* **132** 6498
[37] Tang W, Sanville E and Henkelman G 2009 *J. Phys.: Condens. Matter* **21** 084204
[38] Hui L *et al.* 2015 *Spectrochim. Acta A* **141** 211
[39] Zhao X and Chen M 2011 *Chem. Phys. Lett.* **512** 35
[40] Zhao G J, Northrop B H, Han K L and Stang P J 2010 *J. Phys. Chem. A* **114** 9007
[41] Liu Y H, Lan S C, Zhu C and Lin S H 2015 *J. Phys. Chem. A* **119** 6269
[42] Chou P, Mcmorrow D, Aartsma T J and Kasha M 1984 *J. Phys. Chem.* **88** 370
[43] Liu Y H, Mehata M S and Lan S C 2014 *Spectrochim. Acta A* **128** 280
[44] Lu T and Chen F 2012 *J. Comput. Chem.* **33** 580
[45] Zhao J, Ji S, Chen Y, Guo H and Yang P 2012 *Phys. Chem. Chem. Phys.* **14** 8803
[46] Grabowski Z R, Rotkiewicz K and Rettig W 2003 *Chem. Rev.* **103** 3899
[47] Marcus R A 1968 *Electrochimica Acta* **13** 995
[48] Shahid M and Misra 2017 *J. Photoch. Photobio. A* **335** 190
[49] Johnson E R *et al.* 2010 *J. Am. Chem. Soc.* **132** 6498
[50] Tang W, Sanville E and Henkelman G 2009 *J. Phys.: Condens. Matter.* **21** 084204